Acta Crystallographica Section F
Structural Biology and Crystallization Communications
ISSN 1744-3091

Proteolysis of the type III glutamine synthetase from *Bacteroides fragilis* causes expedient crystal-packing rearrangements

Jason van Rooyen,[a,b]* Hassan Belrhali,[c] Valarie Abratt[b] and B. Trevor Sewell[a,d]

[a]Electron Microscope Unit, University of Cape Town, South Africa, [b]Department of Molecular and Cell Biology, University of Cape Town, South Africa, [c]European Molecular Biology Laboratory, Grenoble, France, and [d]Institute of Infectious Diseases and Molecular Medicine, University of Cape Town, South Africa

Correspondence e-mail: jason@science.uct.ac.za

Received 8 November 2010
Accepted 22 December 2010

This work details the intentional modifications that led to the first structure of a type III glutamine synthetase enzyme (GSIII). This approach followed the serendipitous discovery of digestion caused by an extracellular protease from a contaminating bacterium, *Pseudomonas fluorescens*. The protease only cleaves the GSIII protein at a single site, leaving the oligomer intact but allowing the protein to crystallize in a different space group. This transition from space group $P1$ to space group $C222_1$ is accompanied by improved growth characteristics, more reproducible diffraction and enhanced mechanical stability. The crystallographic analyses presented here provide the structural basis of the altered molecular packing in the full-length and digested crystal forms and suggest modifications for future structural studies.

1. Introduction

The largest of the glutamine synthetase (GS) enzymes, the type III glutamine synthetases (GSIIIs), occur in evolutionarily diverse species (Xu *et al.*, 2003; Goodman & Woods, 1993; Amaya *et al.*, 2005; Southern *et al.*, 1986; Kinoshita *et al.*, 2009). However, until recently only low-resolution structural information existed to describe them (van Rooyen *et al.*, 2006). We have recently determined the first crystal structure of a large (∼1 MDa) GSIII enzyme from *Bacteroides fragilis* and the results (van Rooyen *et al.*, 2011) have helped to explain the evolution of the important GS superfamily and have highlighted several strategies for targeting these divergent enzymes through rational drug design. Our success was greatly facilitated by the serendipitous discovery of proteolysis-mediated changes at the surface of the GSIII dodecamers which allowed the protein to crystallize in a higher symmetry space group. It was from these crystals that the latter structure solution resulted. Here, we detail the discoveries that led to this result and reveal the underlying molecular alterations that are responsible for the substantial changes in crystal packing.

2. Methods and materials

2.1. Protein isolation

Pure recombinant *B. fragilis* GSIII was prepared from an *Escherichia coli* heterologous expression host using a combination of divalent-cation precipitation and affinity chromatography as described previously (van Rooyen *et al.*, 2010).

2.2. Isolation of a bacterial protease

An inoculum of the contaminating bacteria was isolated from crystallization plates which lacked bacteriostatics. Subsequent cultures were grown on Luria–Bertani (LB) agar plates or in 5 ml volumes of LB broth at 294 K without aeration. The bacterial contaminant was identified as *Pseudodomonas fluorescens* following 16s rRNA gene sequencing by Macrogen Inc., Seoul, Republic of Korea. The universal primers F27 (5′-AGAGTTTGATCITGGCT-CAG-3′) and R5 (5′-ACGGITACCTTGTTACGACTT-3′) (Chèneby

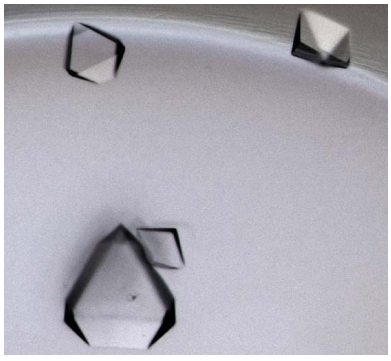

et al., 2000) were used during PCR and sequences were analysed using *BLAST* v.2.2.17 (Altschul *et al.*, 1990).

The culture supernatant (CS) was prepared from a 5 ml culture of *P. fluorescens* grown in LB and incubated at 294 K for 2 d. After centrifugation of the culture for 15 min at 14 000 rev min^{-1} in a desktop centrifuge, the CS was stored at 253 K and used in all subsequent proteolysis experiments.

2.3. Protease-susceptibility assays

Aliquots of 4 mg ml^{-1} GSIII in 15 m*M* imidazole pH 7.1 were mixed with an equal volume of *P. fluorescens* CS (serial doubling dilution in dH_2O) and incubated at 294 K for 16 h. Digestion was halted by the addition of gel-loading buffer and the samples were analyzed by SDS–PAGE. An untreated sample of GSIII was incubated at 294 K for 24 h to serve as a negative control. Enzyme activity was monitored by the gamma-glutamyltransferase assay as modified by Southern *et al.* (1986).

2.4. Identification of proteolysis products

In-gel tryptic digestion and MALDI–TOF mass-spectrometric fingerprinting of the resulting peptides were carried out using established protocols (Rosenfeld *et al.*, 1992). Mass spectra were collected on an ABI 4800 MALDI–TOF/TOF machine in reflection positive mode operating at 20 kV source voltage and 16 kV grid voltage with a 400 ns delayed extraction time. A default calibration was applied and a scan range of 800 to −4000 *m*/*z* was used to collect data with 50 shots per subspectrum and a total of 1000 spectra. Data processing was carried out using *GPS EXPLORER* software from ABI and proteins were identified using the *Mascot* web server.

2.5. Characterization of digested GSIII complex

GSIII protein (10 mg ml^{-1}) digested with *P. fluorescens* supernatant as described above and an undigested control were loaded separately onto a Tosoh PWXL-4000 column pre-equilibrated with 0.1 *M* citric acid/0.05 *M* NaH_2PO_4 pH 5.8 and 100 m*M* KCl at 0.4 ml min^{-1}. The column had previously been calibrated using high-molecular-weight standards from Bio-Rad, 3%(*v*/*v*) acetone and TMV. Identical samples (1 µg) were also mixed with gel-loading buffer without SDS and β-mercaptoethanol for analysis by discontinuous native PAGE (Ornstein, 1964) with 2.5% acrylamide stacking and 4% acrylamide separating gels.

2.6. Crystallization of digested GSIII

Proteolysis was achieved by mixing equal volumes of *P. fluorescens* CS with pure GSIII (6 mg ml^{-1} in the final affinity-chromatography elution buffer; van Rooyen *et al.*, 2010) and incubating for 16 h at room temperature. The digested protein was then reconcentrated and buffer-exchanged (three times to one fifth of the volume) in equilibration buffer using a 100 kDa molecular-weight cutoff Nanosep centrifugal concentrator (Pall Corporation) to give a final concentration of 3.5 mg ml^{-1}. Crystallization was achieved by using the same conditions that had proved to be successful for the full-length GSIII

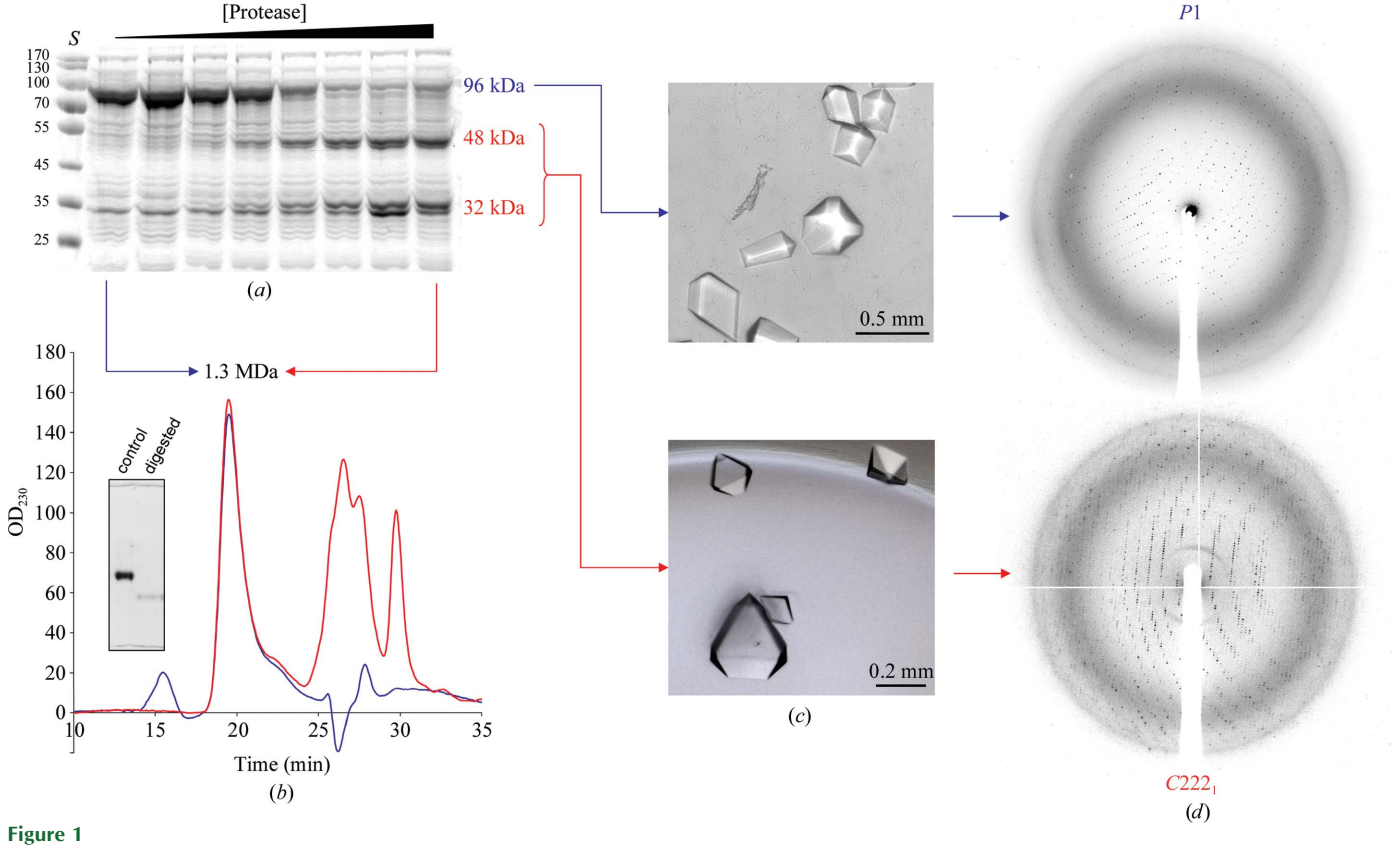

Figure 1
Alternate crystal forms resulting from limited proteolysis of GSIII. (*a*) Coomassie Blue-stained 10% SDS–PAGE gel of the proteolysis products (48 and 32 kDa) resulting from the addition of different concentrations of *P. fluorescens* culture supernatant to semi-pure GSIII (96 kDa). Molecular-weight standards were loaded into the lane marked *S* and their weights are given in kDa on the left. (*b*) Size-exclusion chromatograph of digested (red) and undigested (blue) GSIII. Inset, full-length (control) and digested GSIII were also analysed by native PAGE. (*c*) Crystals of full-length and digested (cross-seeded) GSIII grown under identical conditions. (*d*) Oscillation images (1°) of the full-length (*P*1) and digested (*C*222$_1$) GSIII crystals. Data collection was performed as described in §2.7. The maximum recorded resolution was 2.9 Å and the contrast levels of the images were adjusted for presentation purposes.

Table 1
Data-collection statistics.

Values in parentheses are for the highest resolution shell.

Crystal data		
Space group	$C222_1$	$P1$†
Unit-cell parameters (Å, °)	a = 198.25, b = 203.96, c = 234.59, $\alpha = \beta = \gamma$ = 90.00	a = 141.79, b = 148.30, c = 159.33, α = 115.76, β = 93.65, γ = 115.99
Unit-cell volume (Å^3)	9485663	2574882
Matthews coefficient V_M (Å^3 Da^{-1})	2.41	2.62
No. of molecules in asymmetric unit	6	12
Solvent content (%)	48.99	53.02
Data collection		
Resolution range (Å)	62.87–3.50 (3.69–3.50)	130.0–3.5 (3.69–3.50)
No. of unique reflections	60104 (8687)	123636 (18005)
No. of observed reflections	471192 (68419)	490235 (71612)
Completeness (%)	100	98.3 (98.0)
Multiplicity	7.8	4.0
Signal to noise	11.2 (4.6)	12.3 (4.6)
R_{merge}‡ (%)	20.8 (47.2)	10.9 (32.5)
$R_{p.i.m.}$ (all I^+ and I^-) (%)	7.9 (17.9)	6.3 (18.9)
Wilson B factor (Å^2)	45.0	62.1

† Data were scaled to 3.5 Å resolution to facilitate comparison with the $C222_1$ crystal form, but molecular replacement and rigid-body refinement included data to 3 Å. ‡ $R_{merge} = \sum_{hkl}\sum_i |I_i(hkl) - \langle I(hkl)\rangle| / \sum_{hkl}\sum_i I_i(hkl)$.

protein (van Rooyen *et al.*, 2010) and growth was initiated by cross-seeding with nuclei from crystals of the latter. Further batches of crystals were prepared by streak-seeding equilibrated drops (1.75 mg ml^{-1} digested GSIII) with nuclei from these new crystals. Crystal growth to about 0.1 mm was achieved in 2–4 d.

2.7. Data collection and processing of the full-length GSIII protein

All crystallographic data were collected on the BM14 beamline at the ESRF, Grenoble, France as described in van Rooyen *et al.* (2010). Complete data sets were collected to 3 Å resolution at 100 K from a $P1$ native crystal and a $C222_1$ digested crystal of similar dimensions (0.1 × 0.1 × 0.1 mm) that were preserved under optimized cryo-conditions (Paratone-N oil). A custom-designed low-resolution beamstop developed by the UK MRC–EMBL Grenoble teams was used and allowed low-resolution data set to be collected to 130 Å for the $C222_1$ case; it was fitted during both experiments. In addition, during the characterization of the different crystal forms an HC1b humidity-control device was used to vary the relative humidity (RH) during data collection (Sanchez-Weatherby *et al.*, 2009). MicroRT capillaries (MiTeGen) were also used to initially evaluate room-temperature diffraction from each crystal form.

Initial indexing and evaluation of the data quality were carried out with *iMOSFLM* (Leslie, 2006) and space-group assignments were evaluated with *POINTLESS* (Evans, 2006). Scaling, reduction and merging of the $C222_1$ diffraction data were carried out using *SCALA* (Evans, 2006) within the *CCP*4 suite (Collaborative Computational Project, Number 4, 1994). The final integration, scaling and merging of the $P1$ data was performed using *XDS* (Kabsch, 2010).

2.8. Crystal-packing analysis

The dodecameric biological unit of the digested GSIII structure (PDB code 3o6x; van Rooyen *et al.*, 2011) was used as a search model for molecular replacement of the full-length data using *MOLREP* (Vagin & Teplyakov, 2010) from the *CCP*4 suite (Collaborative Computational Project, Number 4, 1994). The most promising solution was then subjected to rigid-body refinement in *CNS* (Brünger *et al.*, 1998), treating each of the 12 protomers as individual rigid bodies. This maximum-likelihood refinement was carried out over ten cycles with 20 rounds of minimization, each with overall anisotropic B-factor and bulk-solvent corrections, resulting in a decrease in R_{free} from 0.47 to 0.37.

Symmetry-related neighbours within 10 Å of atoms in the asymmetric unit were generated from both the $P1$ and $C222_1$ (van Rooyen *et al.*, 2011) structures using *PyMOL* (DeLano, 2002). Crystal contacts were then identified in *UCSF CHIMERA* (Pettersen *et al.*, 2004) using the CLASH/CONTACT plugin with a van der Waals overlap limit of ≥ -3.5 Å. Additional calculations to ascertain the changes in surface area upon oligomerization and crystallization were carried out in *AREAIMOL* (Collaborative Computational Project, Number 4, 1994; Lee & Richards, 1971) with a solvent probe radius of 1.4 Å.

All molecular renderings were performed in *UCSF Chimera* (Pettersen *et al.*, 2004).

3. Results and discussion

3.1. Limited proteolysis

During the isolation of GSIII (van Rooyen *et al.*, 2010) it was serendipitously discovered that a bacterial contaminant in the protein preparation was secreting a protease that was capable of nicking the protein at a surface-exposed site. Under denaturing conditions, the digested GSIII protein yielded two peptides with masses of around 48 and 35 kDa. Following the isolation of these peptide products using SDS–PAGE, the identity of the larger fragment was confirmed as an N-terminal fragment of GSIII using peptide-fingerprinting mass spectroscopy.

The bacterial contaminant was isolated and cultured. The sequence of its 16s rRNA gene identified it as *P. fluorescens*, which is known to secrete an extracellular protease (Liao & McCallus, 1998). The culture supernatant was tested for activity and the resultant peptide masses matched those seen in the contaminated protein stock (Fig. 1*a*). Further characterization of the protease activity showed that proteolysis by the *P. fluorescens* culture supernatant did not progress to further digestion even after prolonged storage (two weeks) at 277 K. Size-exclusion chromatography confirmed this by showing that the complex remained intact after digestion (Fig. 1*b*), but the higher resolution of native PAGE revealed a slight change in the mass–charge ratio (Fig. 1*b*, inset). However, similar digestions with trypsin yielded the same-sized products after short incubations, but longer timescales resulted in complete digestion of GSIII (results not shown). Estimates of the proteolytic cleavage site near residue 430 were made from the masses of the intact fragments derived from MALDI–TOF mass spectrometry (32 874 and 48 360 Da) and the known GSIII sequence (Hill *et al.*, 1989). It is well known that proteolytic sensitive sites are generally solvent-exposed extended loops and that their mobility is the primary determinant of protease susceptibility (Hubbard, 1998). In keeping with the masses of the fragments, it therefore seemed likely that the cleavage results in the loss of a surface-exposed loop near residue 430.

3.2. Improved crystals

Proteolytic treatment under nondenaturing conditions has become a standard strategy for modifying crystallization behaviour (Newman, 2006). By removing the intrinsically disordered surface loops that contribute significantly towards conformational heterogeneity, the likelihood of a protein crystallizing can be increased. Crystallization of the digested complex was therefore attempted in the hope that the modified GSIII complex might yield higher quality crystals. Crystal

trials of digested GSIII were carried out using the same conditions that proved successful for the full-length enzyme and similar protein concentrations (van Rooyen *et al.*, 2010). Cross-seedings using nuclei from the full-length crystals were able to produce large individual

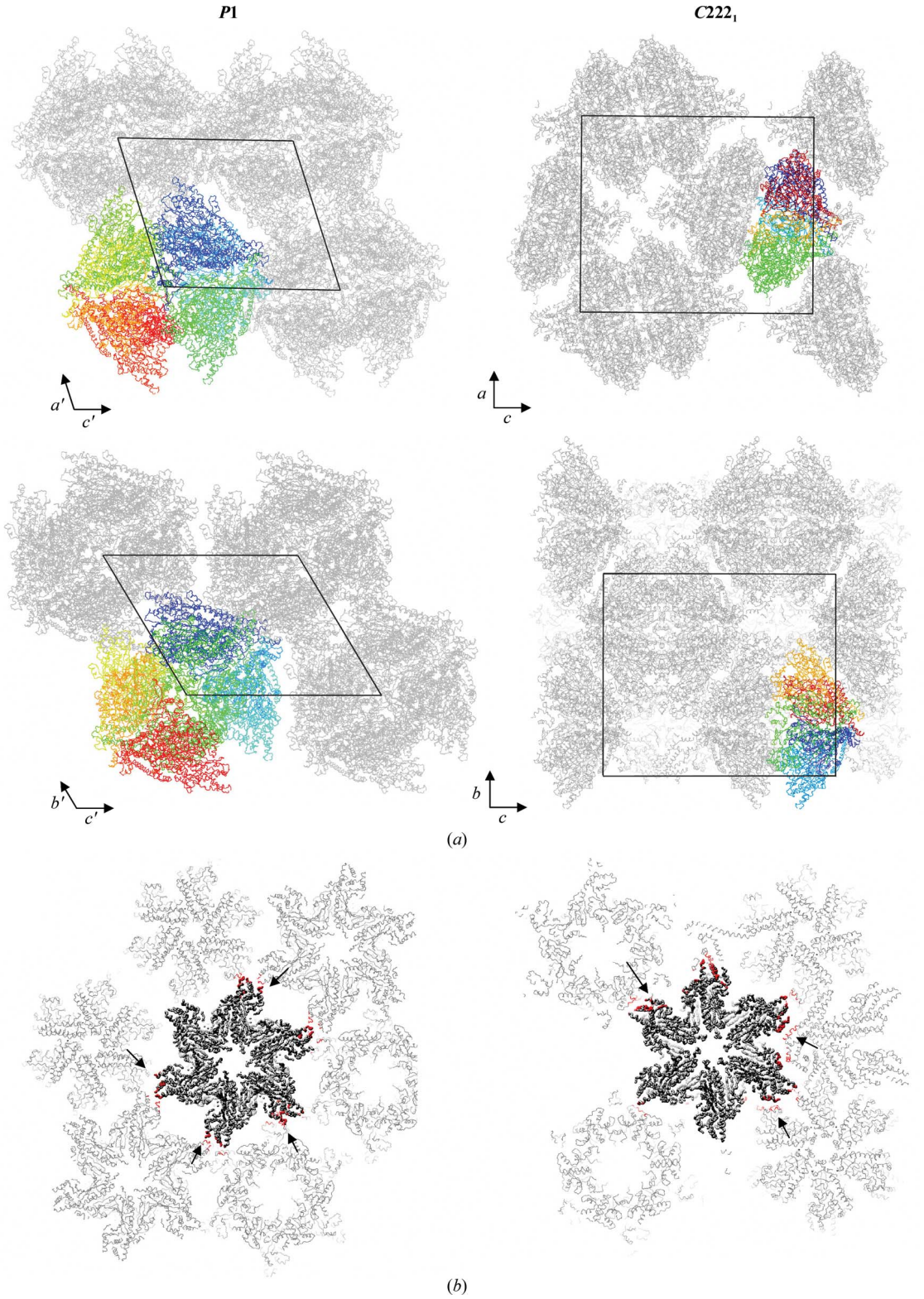

Figure 2
Digestion of a surface-exposed loop leads to improved molecular packing in the higher symmetry crystal form. (*a*) Crystal-packing diagrams comparing the arrangement of dodecamers in the alternate lattices. The unit cell is shown in black and the subunits in the biological asymmetric unit are highlighted in different colours. (*b*) Crystal-contact changes resulting from proteolysis. The GSIII asymmetric unit is shown in thick C^{α}-trace representation and symmetry-related molecules within 10 Å are shown in thin C^{α}-trace representation. Only one ring of the dodecamer in the *P*1 form is shown. Residues of the dodecamer which approach closer than 3.5 Å to symmetry-related neighbouring molecules are highlighted in red. Arrows mark the positions of contacts involving the region of protease susceptibility.

crystals that displayed a clearly different bipyramidal habit after several days of growth (Fig. 1*c*).

Room-temperature experiments showed that the two crystal forms diffracted weakly to 3.5 Å resolution, with the full-length GSIII protein and the digested protein crystallizing in space groups *P*1 and $C222_1$, respectively (Fig. 1*d* and Table 1). At this temperature, the crystals exhibited radiation-sensitivity, only surviving 100 s in the bending-magnet synchrotron beam; the diffraction quality between crystals was somewhat variable but was routinely better for the larger $C222_1$ crystals (Fig. 1*d* and Table 1). The latter crystals also displayed a reversible transition during *in situ* dehydration experiments with the HC1b device. While the *P*1 crystals lost all diffraction upon dehydration below 90% RH, the $C222_1$ crystals regained their upper resolution diffraction limit when returned to 98% RH for 5 min (data not shown). These results confirmed the previously noted fragility of the *P*1 crystals in comparison to the more robust $C222_1$ form, which were less likely to fracture during manual manipulation.

Cryoprotection in standard buffers containing 20% PEG 400 and 25% glycerol resulted in a reduction of the diffraction limit to 7 Å for both crystal forms following flash-cooling in a cryostream (data not shown). It was subsequently determined that these crystals only lost order during the freezing process, as they still diffracted to 3.5 Å at ambient temperature in MicroRT capillary mounts after soaking in 30% glycerol for 15 min. Following a systematic assessment of cryoconditions, Paratone-N oil was found to be the only easily reproducible method of preserving higher resolution diffraction from both the *P*1 and $C222_1$ crystal forms during flash-freezing in the cryostream or in liquid nitrogen.

3.3. Crystallographic identification of the protease-susceptible site

Following the solution of the X-ray crystal structure from the $C222_1$ crystal data (van Rooyen *et al.*, 2011), it has been possible to map the site of proteolytic sensitivity near residue 430 to a region of missing density at the tips of the subunits of the dodecameric GSIII structure. As predicted from its amino-acid sequence, this 33-residue region appears to be disordered; no additional density could be seen in the *P*1 (full-length) electron-density maps and the temperature factors were highest at the ends of the pinwheel arms in the $C222_1$ structure (van Rooyen *et al.*, 2011). The protease-sensitivity and the change in mobility of GSIII seen on native PAGE can therefore be explained by the accessibility and flexibility of this loop region.

3.4. Effects of altered crystal packing

Using the refined 3.5 Å resolution GSIII crystal structure (van Rooyen *et al.*, 2011), it has also been possible to examine the underlying changes that are responsible for the differences in molecular packing following digestion. Although the *P*1 structure was not refined to atomic detail, the results of the molecular-replacement and rigid-body refinement analyses presented here reveal the effects of proteolysis on the molecular contacts between the component dodecamers in the two crystal forms (Fig. 2*a*). The *P*1 crystal form is made up of layers of GSIII dodecamers arranged in a hexagonal fashion in the *ab* plane. These layers then stack on top of each other in an offset manner, with the large flat surfaces of the GSIII conical domes fitting into each other like saw teeth (Fig. 2*a*; *P*1, $a'c'$ and $b'c'$ views). In the $C222_1$ crystals the dodecamers are also arranged in parallel arrays with the principal axes of the GSIII dodecamers aligning with the crystallographic axes (Fig. 2*a*; $C222_1$, *bc* view). However, when viewed from the *ac* plane it can be seen that every alternate layer is composed of parallel arrays of molecules arranged with their sixfold axes tilted in opposite directions from the *c* axis (Fig. 2*a*; $C222_1$, *ac* view).

The predominant packing interface formed by the large domed surface in both crystals is composed of a central hydrophobic stripe which is surrounded on either side by charged residues (van Rooyen *et al.*, 2011). These surfaces are formed by the helical bundles which make up the spokes of the 'pinwheel' arms. It is therefore likely that these surface features are also responsible for the resolution-limiting preferential attachment of GSIII to the carbon support film and air–water interface observed during electron-microscopy studies (van Rooyen *et al.*, 2006).

It can be seen from these analyses that the protease-susceptibility site located at the tips of the pinwheel arms contributes to crystalline packing through the formation of several crystal contacts with neighbouring dodecamers (Fig. 2*b*). In the *P*1 crystal these regions interact primarily with adjacent dodecamers in the same layer. However, after proteolysis the nature of the interaction changes, resulting in a greater number of contacts between the molecules of the asymmetric unit and adjacent dodecamers (Fig. 3). The total

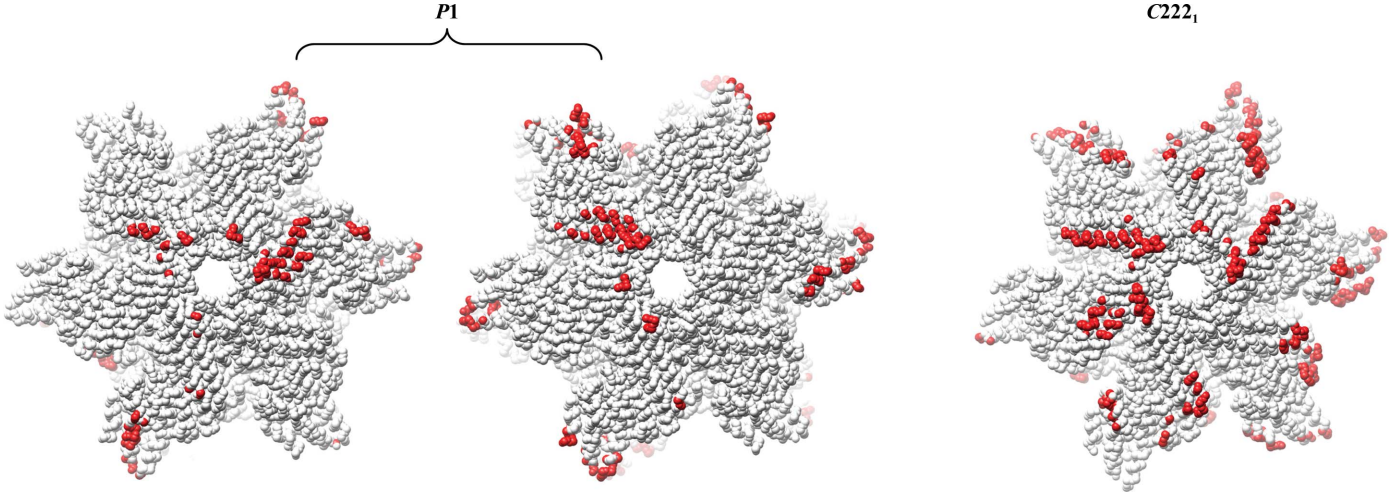

Figure 3
Increase in crystal-packing contact areas following digestion. Axial views of the GSIII hexamers (van Rooyen *et al.*, 2011) comprising the asymmetric units of both crystal forms are shown in thick C^{α}-trace representation. Residues which approach closer than 3.5 Å to symmetry-related neighbouring molecules are coloured red.

surface area buried upon crystallization increases from 2771 Å^2 in the *P*1 crystal form to 5056 Å^2 in the $C222_1$ crystal form (excluding the inter-ring interactions), *i.e.* there is almost a doubling of packing-contact area. These changes to the crystalline order therefore explain the improved mechanical stability and growth characteristics of the orthorhombic crystals.

In conclusion, the GSIII enzyme possesses a surface-exposed flexible loop, the cleavage of which by an extracellular protease from *P. fluorescens* does not alter the oligomeric structure but does change the surface properties. This modification is sufficient, under the same crystallization conditions, to alter the crystal-packing interactions and leads to the formation of a crystal form with higher symmetry, improved mechanical properties and enhanced growth characteristics. We propose that the truncation of this region by limited proteolysis or genetic manipulation will facilitate the solution of many more GSIII enzymes. The accessibility, low cost and specificity of the low-temperature protease from *P. fluorescens* may also prove useful to experimentalists wishing to modify other proteins in preparation for crystallization.

This work was supported by the National Research Foundation (NRF) of South Africa. Synchrotron access was provided by the European Molecular Biology Laboratory. JvR acknowledges PhD scholarships from the NRF, University of Cape Town and the Cape Biotech Trust. We also gratefully acknowledge the efforts of Mr L. Motlogelwa, Ms A. Thorpe and Ms C. Williams in identifying the *P. fluorescens* bacterium.

References

Altschul, S. F., Gish, W., Miller, W., Myers, E. W. & Lipman, D. J. (1990). *J. Mol. Biol.* **215**, 403–410.
Amaya, K. R., Kocherginskaya, S. A., Mackie, R. I. & Cann, I. K. (2005). *J. Bacteriol.* **187**, 7481–7491.
Brünger, A. T., Adams, P. D., Clore, G. M., DeLano, W. L., Gros, P., Grosse-Kunstleve, R. W., Jiang, J.-S., Kuszewski, J., Nilges, M., Pannu, N. S., Read, R. J., Rice, L. M., Simonson, T. & Warren, G. L. (1998). *Acta Cryst.* D**54**, 905–921.
Chèneby, D., Philippot, L., Hartmann, A., Hénault, C. & Germon, J. (2000). *FEMS Microbiol. Ecol.* **34**, 121–128.
Collaborative Computational Project, Number 4 (1994). *Acta Cryst.* D**50**, 760–763.
DeLano, W. L. (2002). *PyMOL*. http://www.pymol.org.
Evans, P. (2006). *Acta Cryst.* D**62**, 72–82.
Goodman, H. J. & Woods, D. R. (1993). *J. Gen. Microbiol.* **139**, 1487–1493.
Hill, R. T., Parker, J. R., Goodman, H. J., Jones, D. T. & Woods, D. R. (1989). *J. Gen. Microbiol.* **135**, 3271–3279.
Hubbard, S. J. (1998). *Biochim. Biophys. Acta*, **1382**, 191–206.
Kabsch, W. (2010). *Acta Cryst.* D**66**, 125–132.
Kinoshita, S., Isu, S., Kaneko, G., Yamada, H., Hara, T., Itoh, Y. & Watabe, S. (2009). *Mar. Genomics*, **2**, 103–111.
Lee, B. & Richards, F. M. (1971). *J. Mol. Biol.* **55**, 379–400.
Leslie, A. G. W. (2006). *Acta Cryst.* D**62**, 48–57.
Liao, C. H. & McCallus, D. E. (1998). *Appl. Environ. Microbiol.* **64**, 914–921.
Newman, J. (2006). *Acta Cryst.* D**62**, 27–31.
Ornstein, L. (1964). *Ann. N. Y. Acad. Sci.* **121**, 321–349.
Pettersen, E. F., Goddard, T. D., Huang, C. C., Couch, G. S., Greenblatt, D. M., Meng, E. C. & Ferrin, T. E. (2004). *J. Comput. Chem.* **25**, 1605–1612.
Rosenfeld, J., Capdevielle, J., Guillemot, J. C. & Ferrara, P. (1992). *Anal. Biochem.* **203**, 173–179.
Sanchez-Weatherby, J., Bowler, M. W., Huet, J., Gobbo, A., Felisaz, F., Lavault, B., Moya, R., Kadlec, J., Ravelli, R. B. G. & Cipriani, F. (2009). *Acta Cryst.* D**65**, 1237–1246.
Southern, J. A., Parker, J. R. & Woods, D. R. (1986). *J. Gen. Microbiol.* **132**, 2827–2835.
Vagin, A. & Teplyakov, A. (2010). *Acta Cryst.* D**66**, 22–25.
van Rooyen, J. M., Abratt, V. R., Belrhali, H. & Sewell, B. T. (2010). *Protein Expr. Purif.* **74**, 211–216.
van Rooyen, J. M., Abratt, V. R., Belrhali, H. & Sewell, B. T. (2011). Submitted.
van Rooyen, J. M., Abratt, V. R. & Sewell, B. T. (2006). *J. Mol. Biol.* **361**, 796–810.
Xu, J., Bjursell, M. K., Himrod, J., Deng, S., Carmichael, L. K., Chiang, H. C., Hooper, L. V. & Gordon, J. I. (2003). *Science*, **299**, 2074–2076.